Fundamental study of multi-track friction surfacing deposits for dissimilar aluminum alloys with application to additive manufacturing

Soujon, Malte; Kallien, Zina; Roos, Arne; Zeller-Plumhoff, Berit; Klusemann, Benjamin

Published in:
Materials and Design

DOI:
10.1016/j.matdes.2022.110786

Publication date:
2022

Document Version
Publisher's PDF, also known as Version of record

Materials & Design 219 (2022) 110786

Contents lists available at ScienceDirect

Materials & Design

journal homepage: www.elsevier.com/locate/matdes

Fundamental study of multi-track friction surfacing deposits for dissimilar aluminum alloys with application to additive manufacturing

Malte Soujon [a,c], Zina Kallien [a,*], Arne Roos [a], Berit Zeller-Plumhoff [b], Benjamin Klusemann [a,c]

[a] Institute of Materials Mechanics, Helmholtz-Zentrum Hereon, Max-Planck-Straße 1, 21502 Geesthacht, Germany
[b] Institute of Metallic Biomaterials, Helmholtz-Zentrum Hereon, Max-Planck-Straße 1, 21502 Geesthacht, Germany
[c] Institute of Product and Process Innovation, Leuphana University of Lüneburg, Universitätsallee 1, 21335 Lüneburg, Germany

HIGHLIGHTS

- Overlap and behavior on edges are investigated for multi-track friction surfacing.
- Defect volume distribution is extensively studied via micro computed tomography.
- Post-processing via hybrid friction diffusion bonding consolidated defects.
- Defect-free structure underlines feasibility as solid state AM techology.

GRAPHICAL ABSTRACT

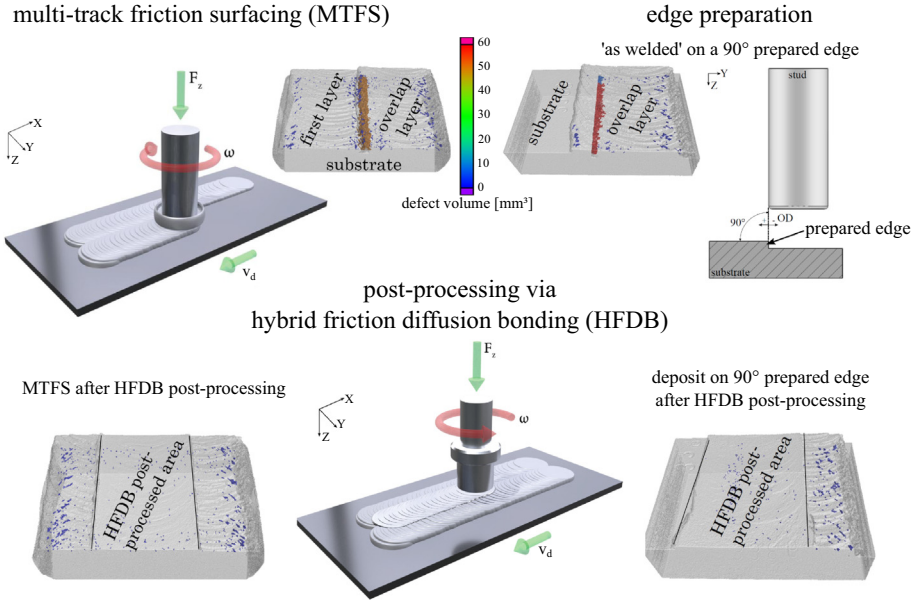

ARTICLE INFO

Article history:
Received 16 March 2022
Revised 23 May 2022
Accepted 24 May 2022
Available online 29 May 2022

Keywords:
Multi-track friction surfacing
Hybrid friction diffusion bonding
microCT
Defect analysis
Tensile properties
Additive manufacturing

ABSTRACT

Friction surfacing is an emerging solid-state coating technology based on frictional heat induced plastic deformation at the tip of a consumable metallic stud that allows to deposit layers with a fine-grained recrystallized microstructure at temperatures below the melting point. The generation of sound, defect-free metallurgical joints between multiple adjacent overlapping friction surfacing deposits, also referred to as multi-track friction surfacing, from dissimilar aluminum alloys is the focus of this experimental work. An extensive volumetric defect analysis is carried out for various overlap configurations, including post-processing strategies in order to assess the inter-track bonding integrity using microscopic characterization techniques and micro-computed tomography. The effect of layer arrangement and overlap distance on the volumetric defect formation in both inter-track and layer-to-substrate interface is quantified and discussed. Post-processing via hybrid friction diffusion bonding process demonstrates a significant reduction in defect volume ratio, proving higher material efficiency. The gained knowledge was used to successfully build a multi-track multi-layer friction surfacing stack, demonstrating the

* Corresponding author.
E-mail address: zina.kallien@hereon.de (Z. Kallien).

https://doi.org/10.1016/j.matdes.2022.110786

suitability of this process for large-scale additive manufacturing components. The subsequent mechanical analysis reveals excellent homogeneous isotropic tensile properties of the additive structure in the range of the base material tensile strength.

1. Introduction

The Friction Surfacing (FS) process, a solid state coating technique for metals, has gained attention due to its potential of joining dissimilar materials [1]. During FS, a stud as consumable material experiences a rotational speed and is pressed with a defined axial force onto a substrate material. At the interface, frictional heat is generated and the tip of the stud plasticizes. A relative translational movement enables the deposition of the plasticized consumable material on the substrate. The deposited material typically shows a fine-grained recrystallized microstructure [2]. Due to the solid state nature of the process, the heat input is lower compared to fusion-based techniques [3], where the specific energy that is necessary to enable the deposition depends on the materials to be processed [4]. Main process parameters are the applied axial force, rotational speed and translational speed, which need to be optimized in order to achieve high-quality deposits [5]. Apart from other aspects related to FS, the influence of these three parameters on the process behavior is summarized in the comprehensive review by Gandra et al. [1].

The FS process was first mentioned in a patent by Klopstock and Neelands [6] in 1941. Being a discontinuous process, the geometry of the resulting FS layer, i.e. length and width, is mainly limited by the dimensions of the used stud and the involved material partners, in particular related to flow behavior and the present heat conduction. The process is feasible for various similar and dissimilar combinations, e.g. deposition of aluminum on steel [5,7]. For dissimilar material combinations with significantly different physical properties, such as titanium and aluminum, hybrid approaches are also developed, e.g. FS assisted by friction stir welding [8]. In order to coat larger areas, it is necessary to implement FS in multiple adjacent overlapping FS tracks. In the following, this approach is named multi-track friction surfacing (MTFS).

Only few studies address the technique of MTFS, since the main work on FS concentrates on single layer deposition. A remaining challenge is that the deposit shows some unbonded regions at the edges, which is characteristic for a FS layer. Puli and Ram [9] reported that sufficient frictional contact between the previously deposited track and the stud while depositing the next layer is necessary to achieve sound metallurgical inter-track bonding. Any volumetric defect can drastically reduce the properties of the coating and its application, e.g. when a certain strength or corrosion resistance is required [1,9]. Additionally, the authors [9] showed that machining of the unbonded regions improves the inter-track bonding. Furthermore, by properly positioning the stud with a defined gap to the edge of the first track, a sound inter-track bonding could be achieved for AISI 440C martensitic stainless steel over low carbon steel [9]. The overlap was derived based on a series of experiments in order to achieve sufficient frictional contact with the edge of the previously deposited track. In this regard, the optimum overlapping distance (OD) varies depending on the material, layer thickness and diameter of the stud. A comparable approach for the deposition of 1C-17Cr martensitic stainless steel on low carbon steel was reported by Shinoda et al. [10], where the effect of four different edge geometries of the previous deposited layer on the inter-track bonding was investigated. A round edge preparation led to a low-defect and sound metallurgical inter-track bonding. Furthermore, a significant influence of the OD on the bonding properties was shown. The cross-sectional area of the overlapping deposits was observed to increase with increasing OD. Additionally, due to the different edge preparations, the edges that had to sustain increasing pressure experienced plastic deformation of the layer edge. Apart from that, the pressure between stud and substrate became progressively weaker, resulting in incomplete bonding and defect formation at the layer-to-substrate (LTS) interface [10].

Hanke et al. [11] reported void-free MTFS coatings for three layers of Cr60Ni40 on Nimonic 80A substrate where the offset between the layers was equal to the radius of the consumable studs. The multiple overlapping layers showed the same microstructure as single layer deposits. Further investigations on MTFS for aluminum for various overlapping ratios were conducted by Tokisue et al. [12,13]. The influence of overlapping side, i.e. advancing side (AS) or retreating side (RS), was investigated, where the overlapping layer was tending to incline to the previous layer independent from applied overlapping side. Unbonded edges, also referred to as cold laps, were observed in the first layer and the overlapping layer. However, by depositing the second layer, the unbonded material of the first layer, depending on the overlapping side, was consolidated. The hardness distribution was relatively homogeneous and no clear interface between the deposited layers could be identified [12].

A few studies showed the successful deposition of two [14], three [15,16] or even more FS layers [17] on top of each other, also known as multi-layer friction surfacing (MLFS) or friction surfacing layer deposition (FSLD), proving the feasibility of the process for additive manufacturing (AM). In this regard, MLFS/FSLD represents a solid state layer deposition (SSLD) technology. Abdelall et al. [18] successfully employed FS as hybrid AM approach by combining MLFS and CNC machining. The combination of MLFS and MTFS would allow larger solid-state AM structures, being more independent from the dimensions of one single FS layer, which is still limited by the stud dimensions. With regard to this aspect, the literature is very scarce. Dilip et al. [19] successfully performed multi-track multi-layer FS (MTMLFS) from mild steel using a construction scheme that generates a pyramidal structure. After depositing the first track, the unbonded material on the RS was machined off. Before depositing the next track, the stud was positioned with a small gap (0.2 mm) to the machined edge of the previously deposited track. This type of layer arrangement intend to consolidate the volumetric defects at the inter-track interfaces through subsequent layer deposition. The results from Dilip et al. [19] have shown sound inter-track and inter-layer bonding with tensile properties comparable to standard wrought mild steel.

The present study focuses on the systematic investigation of inter-track bonding for varied overlapping side and OD as well as layer edge preparation in MTFS for possible AM application. For that purpose, extensive defect analysis is performed using optical microscopy and micro-computed tomography. For the first time, hybrid friction diffusion bonding (HFDB) as promising post-processing technology for FS was investigated to improve layer-to-substrate (LTS) and layer-to-layer (LTL) bonding. HFDB is a solid state joining process combining advantages of friction stir welding and diffusion bonding [20]. The process is characterized by short process cycles and is comparable to FS, but uses a non-consumable tool, which does not blend or penetrate the material.

The general idea of using HFDB as post-processing technique is based on the forging principle of this process. In this regard, the intention is to consolidate the volumetric defects in the overlapping area and the LTS-interface by subsequently applying pressure and deformation, in order to ensure sufficient inter-track bonding across MTFS deposits. In addition, a MTMLFS structure was generated with the most promising layer arrangement and overlap parameter set in order to prove the feasibility for AM. Furthermore, this small AM demonstrator is used to extract specimens for mechanical characterization. The knowledge gained by this study allows to give practical advice for the successful coating of wider areas as well as enabling large AM structures by FS.

2. Experimental methods

2.1. Welding equipment and materials

The experiments of the present study were performed at a special purpose friction welding system (RAS, Henry Loitz Robotik, Germany) providing a working area of 0.5 m × 1.5 m. The system allows forces up to 60 kN, torques up to 200 Nm and rotational speeds up to 6000 rpm. In order to perform the investigation of MTFS, two dissimilar industrial wrought aluminum alloys were selected. AA 5083-H112 as consumable stud material (125 mm length, 20 mm diameter) was deposited on AA 2050-T84 substrates (300 mm length, 130 mm width, 12.5 mm thickness). The surface of the substrate plates was ground with P100 sandpaper and afterwards cleaned with acetone and compressed air.

2.2. Multi-track friction surfacing

The FS process is generally divided into two phases. First, the consumable stud is positioned above the substrate and the plasticizing phase is initiated by spinning up the stud to a defined rotational speed and applying an axial force. As a result, the stud is pressed onto the substrate material and frictional heat is generated, which causes thermal softening, deformation and plasticizing of the consumable material. Consequently, a plasticized region is generated with new metallurgical conditions and shape at the tip of the stud [21]. The deposition phase starts by applying a relative translational movement between the stud and the substrate. For the equipment used in this study, all FS depositions were performed force-controlled. The excess softened stud material, which is pressed out of the stud diameter region, creates an ascending flash around the consumable stud and promotes cold lap formation on both AS and RS of the deposited layer [22]. Once the programmed end position is reached or the entire stud is consumed, the process ends by lifting the remaining stud. Each layer of MTFS follows the principle of FS. Fig. 1 gives a schematic of the MTFS process. All experiments were performed at room temperature, including the subsequent deposition of additional layer, i.e. the previous FS layer could cool down to room temperature before an additional deposition was initiated.

The used (constant) process parameters for plasticizing and deposition phase are presented in Table 1. A higher rotational speed allows faster initial plasticizing of the stud material. In the deposition phase, a lower rotational speed and a comparably low translational speed was used, in order to generate layers with approximately 2 mm thickness. The resulting deposit geometry, i.e. thickness and width, is a direct result of the process parameters as well as the temperature [23,24].

For the deposition of the overlapping layer, the OD, defining the distance between the stud's edge and the edge of the already deposited layer, was varied between −1 mm and 3 mm. A negative OD refers to positioning the stud away from the previously deposited FS track and a positive OD towards it, see Fig. 2a. The overlapping side (AS or RS) of the overlapping layer was also varied. In addition, possible preparations of the previously deposited layer, i.e. different edge preparations that could be advantageous for the inter-track bonding properties were investigated using a specially designed substrate, see Figs. 2b and c. The special substrates are designed with six edge preparations in total, whereby three different variations are used for both AS and RS overlap. Two typical edge preparations, i.e. right-angle and outward bevelling, see Fig. 2c, are achieved by machining. For the outward bevelling, five different angle variations are used, ranging from 15° to 75° in 15° steps. The height of the edges is 2.5 mm, which is approximately the average height for a single layer deposition with the presented process parameters.

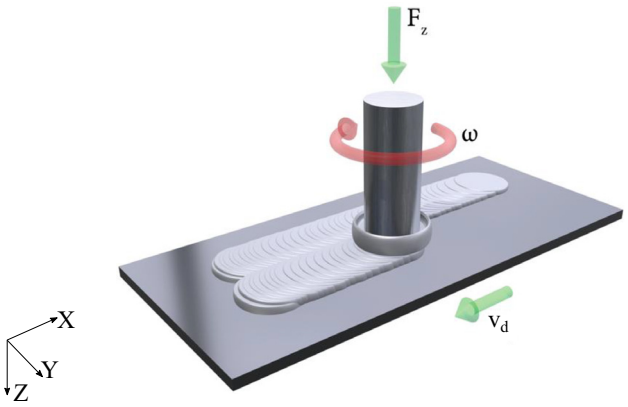

Fig. 1. Schematic of multi track friction surfacing (MTFS) process of the overlapping layer at defined rotational speed ω, axial force F_z and translational travel speed v_d.

2.3. Hybrid friction diffusion bonding

HFDB was developed and invented in 2006 [20] and is a solid state process using the combination of friction and diffusion principles to bond similar or dissimilar materials. Initially, thin sheets and foils were joined by HFDB, where the tool leads to frictional heat and pressure, resulting in activation of diffusion processes enabling a metallic bond [20,25]. The HFDB process follows a similar procedure like the FS process. First, the HFDB tool is positioned above the surface that is supposed to be treated. The tool experiences a rotational speed and is pressed onto the surface until a defined plunge depth is reached. A relative translational speed between rotating tool and surface is superimposed. The HFDB process is performed position-controlled keeping the preprogrammed plunge depth constant. Since the plunge depth of the HFDB tool has a direct influence on the resulting applied axial process force, it is necessary to control the plunge depth in order to keep the resulting axial HFDB process force constant during all HFDB post-processing operations for later assessment. Due to the fact that the irregularities or roughness of the MTFS tracks varies depending on the overlap configuration, especially in the overlapping area, the plunge depth is adjusted individually for each process within a range of 0.1 mm to 2 mm. Consequently, multiple HFDB processes at individually adjusted plunge depths were applied on the generated MTFS tracks and their interface in order to achieve the intended final axial force of approximately 15 kN. For the first HFDB post-processing passes, the plunge depth was set to lower values in order to initially achieve a more even surface for the subsequent post-processing cycles. For the following passes, the even surface allows a planar contact to the HFDB tool and the plunge depth was increased until the intended axial force of 15 kN was achieved. Typically, three HFDB processes were per-

Table 1
Process parameters employed during the two phases in friction surfacing.

stud/substrate	plasticizing			layer deposition		
	axial force	rotational speed	initial shortening	axial force	rotational speed	translational speed
AA5082-H112/AA2050-T84	8 kN	1500 rpm	0.85 mm	8 kN	800 rpm	4 mm/s

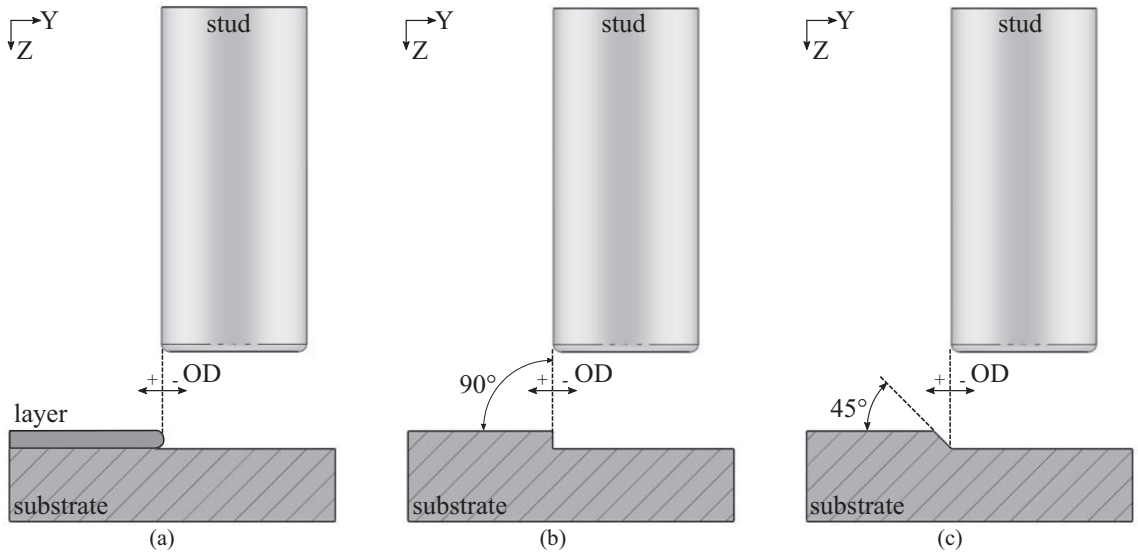

Fig. 2. Schematic representation of OD for positioning the consumable stud for unmachined MTFS deposits (a) and for MTFS deposits on varying edge preparations, e.g. 90° (b) and 45° edge (c).

formed on the MTFS deposits' interface. This procedure allows a comparable and reproducible post-processing, since all structures experience similar process forces during post-processing. The HFDB process ends with the retraction of the tool. The parameter set used for HFDB post-processing is summarized in Table 2. The tool used for HFDB has a 22 mm diameter and consists of quenched and tempered steel (X2NiCoMo18-9–5) with a slightly convex surface (0.5 mm) and a spiral groove in the contact surface, see Fig. 3b. The direction of rotation is determined in such a way, that the plasticized material is transported through the spiral groove towards the tool center. This results in the necessity for a counterclockwise rotation of the tool during this process, where FS was performed in clockwise rotation, see Figs. 1 and 3. Since the HFDB process travel direction is the same as for the FS deposition, AS and RS are transposed between both processes. This was kept constant for all performed experiments of this study. However, in the following, the AS/RS denomination for the final structure is defined by the FS process. An example of a HFDB post-processed MTFS deposit is given in Fig. 3c. The effect of the HFDB process as possible post-processing technology was investigated for variation of OD, overlapping side and edge preparation.

2.4. Multi-track multi-layer friction surfacing

Due to MTFS, the area that can be coated with FS is no longer limited to the diameter of the consumable stud. For the combination of MTFS and MLFS, two approaches are investigated.

One approach follows a pyramid-style construction as presented by Dilip et al. [19] for mild steel. In this approach, layer depositions are performed directly on the overlapping region of the previously deposited layers in order to achieve a consolidation of this region. Each layer overlaps the AS of the previous layer with an OD of 2 mm with its RS. In order to ensure stable plasticizing conditions, the starting area of the underlying layers is preground due to the irregularity and roughness in the overlapping area, before the middle and top layers are deposited.

The other approach of generating MTMLFS deposits aims to obtain an optimized height/width ratio by applying a block-style construction. This means that the same amount of layer material can be used to achieve equal heights and less area is required on the substrate. Additionally, a clearly defined overlapping area can be achieved. Fig. 4 shows the general process of this scheme[1]. In the first step, a MTFS deposit is generated onto the substrate, with the second layer overlapping the first layer with its RS and an OD of 2 mm. Contrary to the pyramid-style construction, it is intended to consolidate the volumetric defects through subsequent HFDB processes. Therefore, the entire surface is then HFDB post-processed, mainly to consolidate the volumetric defects in both the overlapping area and the LTS/LTL interface and to obtain an even surface for subsequent FS processes. The average number of HFDB processes, which were applied to two overlapping layer, was 23 in order to achieve the intended force of 15 kN during post-processing. The parameters for the FS and HFDB processes are presented in Tables 1 and 2, respectively. This procedure is repeated four times to ensure that sufficient material is deposited for metallurgical and mechanical characterization. In the last step, the entire MTMLFS deposit is machined to an almost defect-free structure using CNC machining as can be seen in Fig. 7a.

2.5. Defect analysis

In order to analyze the volumetric defect formation in the generated MTFS deposits, specimens are extracted each with a length of 30 mm, after steady-state deposition condition are given.

[1] The overlapping deposit was initiated with an offset to the already deposited layer in order to achieve a stable plasticizing of the consumable material without contact to previously deposited layer material.

Table 2
Process parameter for HFDB post-processing.

layer material	plunge depth	rotational speed	translational speed	intended axial force
AA5083-H112	0.1 mm - 2 mm	1500 rpm	5 mm/s	15 ± 5 kN

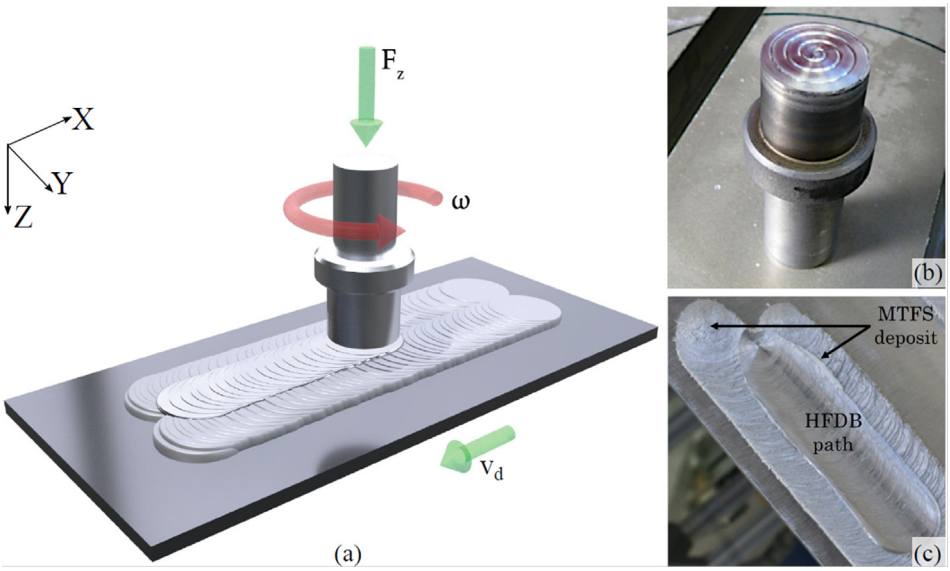

Fig. 3. Schematic principle of HFDB on a MTFS structure (a), HFDB tool (b) and example of HFDB post-processed overlapping area of a multi-track friction surfacing deposit (c).

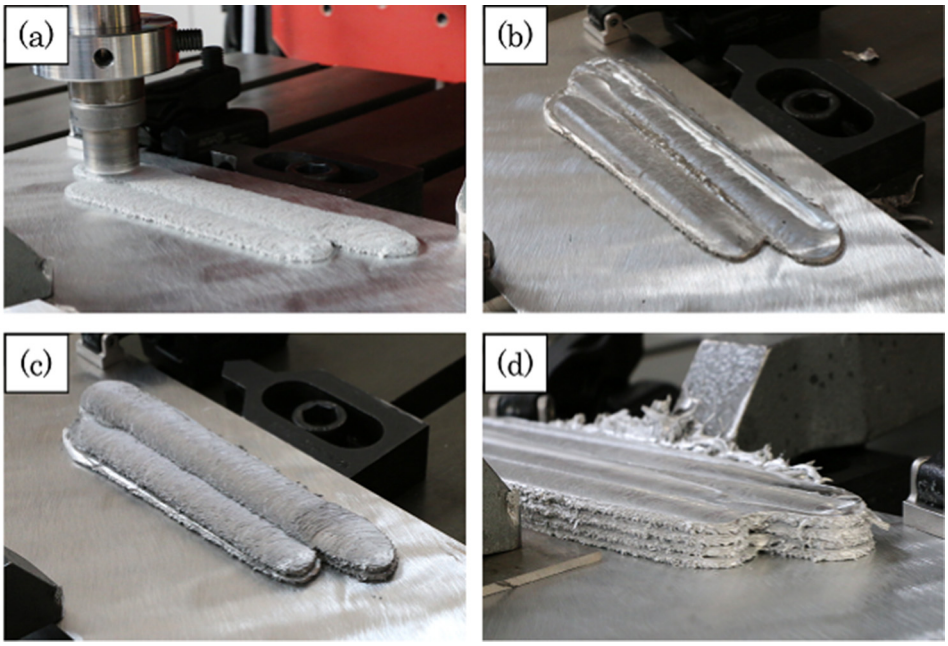

Fig. 4. Manufacturing process of multi-track multi-layer friction surfacing deposit following the block-style deposition scheme, with multiple HFDB processes applied in-between each friction surfacing deposit. For the first stage, two layers are deposited next to each other (a) and multiple HFDB processes are applied to the surface (b) before the next two layers are deposited on top (c), which experience HFDB post-processing as well. In total, four layers are deposited where each consists of two deposits next to each other (d).

Depending on the subsequent investigation procedure, the samples are additionally ground and polished. Microscopic analysis of the cross-sections was performed using a light optical microscope (VHX-6000, Keyence, Germany). X-ray micro-computed tomography (microCT) scans for volumetric defect analysis are conducted using a standard laboratory micro-focus X-ray system (Y.Cougar SMT, YXLON International GmbH, Germany). The parameters are optimized according to the guidelines presented in [26,27]. MicroCT scan settings of 120 kV and 70 µA are used, with image acquisition of 0.93 h per scan and 1080 projections in a full rotation

(360°). The source voltage and current values are based on parameter studies conducted for the used material composition and thickness of the specimen. An 1 mm thick copper (Cu) filter is placed on the beam source to avoid beam-hardening artifacts in the resulting images. Table 3 summarizes the employed parameters for the microCT measurements.

The reconstruction is performed with VGStudio MAX 2.2 (Volume Graphic GmbH, Germany), using the Feldkamp reconstruction algorithm [28], yielding a final voxel size of 48 μm. The data is then analyzed using the software VGStudio Max 3.2 (Volume Graphics GmbH, Germany) including the additional porosity/inclusion analysis module for defect analysis. Figs. 5 and 6 show microCT images for an unmachined MTFS deposit as well as for a MTFS deposit on a prepared edge, respectively, in three different orientations and in a transparent 3D rendering.

The volumetric defect analysis is performed as described in the following. After importing the volume data, an accurate segmentation of the object boundaries is performed in order to separate the material from the exterior air as well as defects. The segmentation is achieved by applying an advanced automatic surface determination using module available in VGStudioMax. To ensure that the surface is accurately defined, the advanced mode with the "remove particles" and "all voids" settings has to be activated. Consequently, as the command implies, all voids and particles inside the object as well as the noise outside the object are removed and not considered as surface areas, regardless of their size. Since the area to be analyzed is mainly concentrated on the LTS-interface and within the deposited layers, a region of interest (ROI) has to be created in order to define the analysis volume, see Figs. 5 and 6. In this regard, the analyzed material volume can be kept similar for all specimens, which allows better comparison of the results. The ROI is positioned in the center of each specimen with a length of 28 mm and a distance of 1 mm to both sides in order to avoid edge artifacts. Both, the width and height of the ROI is adjusted for each specimen in such a way that the entire layer or MTFS deposit is placed inside the ROI. To ensure that all defects are identified, the ROI is positioned 0.1 mm below the LTS-interface. The defect analysis is performed using the VGDefX algorithm.

According to Du Plessis et al. [29], the typical minimum defect size that can be identified in microCT-images has to be at least 3 voxels wide, i.e. in 3D at least 27 voxel ($3 \times 3 \times 3$). Taking this general rule into account, the minimum detectable defect size for this analysis is 144 μm (3×48 μm voxel size). Therefore, all defects with a volume $\geq$0.003 mm^3 are quantifiable. One important value for comparing different multi-track overlapping strategies and post-processing techniques is the defect volume ratio, which is determined as ratio of defect volume and analyzed material volume from the ROI.

2.6. Tensile testing

In order to investigate the tensile properties of the deposited layer material after HFDB post-processing, specimens for microflat tensile testing (MFTT) are extracted horizontally to the interface plane in different positions and orientations within the MTMLFS structure according to Fig. 7c. In each position (A-I) four MFTT specimens are extracted along the stack height, each having the dimensions shown in Fig. 7b. The specimens are uniformly distributed with a gap of 0.3 mm to each other and a distance of approximately 1 m to the surface and substrate to provide sufficient space for electrical discharge machining (EDM). By extracting the MFTT specimens using EDM, a precise sectioning distance as well as a traceable positioning of the specimen can be achieved, which is necessary for determining a possible gradient in mechanical properties within the MTMLFS structure [30]. In addition, the EDM process provides a constant surface roughness of around 2.5 μm. The tensile tests were performed on a tensile testing machine (Zwick/Roell, Germany) with a 5 kN load cell at a constant testing velocity of 0.1 mm/min. The displacement is measured by a laser extensometer (Fiedler Optoeletronik GmbH, Germany). Additionally, high resolution microCT scans were conducted in the gauge length of the MFTT specimens. The scans were conducted at the Manchester Imaging Branchline (I13-2), at Diamond Light Source UK, using a pink beam at a mean energy of 27 keV, an exposure time of 140 ms and 2500 projections. For the high-resolution camera detector pco.edge 5.5 (PCO AG), two objective variants were used for different image resolutions: one lens with 4× magnification, a pixel size of 1.625 μm and a resolution of 3.54 pixel and another lens with 8× magnification, a pixel size of 0.8125 μm and a resolution of 1.974 pixel.

3. Results & Discussion

3.1. Defect analysis

3.1.1. MTFS deposits

Effect of overlapping distance and side

For the investigation of the volumetric defect formation in the overlapping area as well as at the LTS-interface, MTFS structures were generated by depositing two layers next to each other, see Section 2. Multiple experiments were performed in order to investigate different overlap configurations. Therefore, overlapping side, i.e. overlap with AS or RS, and OD were varied as well as the effect of HFDB post-processing technique was investigated.

Fig. 8 displays the measured defect volume ratios of the individual unmachined MTFS deposits, i.e. without any post-processing, depending on the OD and the overlapping side. For RS overlap, the maximum defect volume ratio is measured at 0 mm OD (1.83 %) and the minimum at 2 mm OD (0.98 %), see Fig. 8. Due to partly non-closed regions in the overlapping area, leading to high defect volume ratios, as well as high lateral force fluctuations on the stud during the deposition process, RS overlap at an OD of 0 mm and below has to be classified as an undesirable layer deposition. In the current study, for RS overlap with OD 2 to 3 mm, the lowest volumetric defect ratios were obtained. For AS overlap, similar trends are observed, however, for an OD of 2 mm, a comparatively high defect volume ratio is obtained. The minimum defect volume ratio for AS overlap, which is lower than all the results obtained for RS overlap, is found for an OD of 3 mm.

To analyze the defect volume distribution in detail, exemplary samples showing the maximum and minimum defect volume ratios are visualized in Fig. 9. A uniform volumetric defect distribution for the first layer of all generated MTFS deposits is observed. Stable process parameters and deposition conditions are present for the deposition of the first layer. The unbonded layer edges are the main positions where volumetric defects are located. Additionally, some small defects in the main bonding area of the LTS-interface in the range of the minimum detectable defect volume (0.003 mm^3) are identified. The generated unmachined MTFS deposits exhibit a distinct volumetric defect formation in the overlapping area, forming a kind of "tunnel defect" that represents the majority of the total defect volume. This "tunnel defect" is reduced with increasing OD, for both AS and RS overlap, Fig. 8. However, an increasing defect formation occurred in the main bonding area of the overlapping layer with increasing OD, resulting in a larger area of incomplete bonding in the LTS-interface, especially for RS overlap, see Fig. 9. The same applies for the cold laps of the overlapping layers, which increase with increasing OD, regardless of the overlapping side. This phenomenon is apparently independent of the deposited material, as also observed for martensitic stainless steel

Table 3
MicroCT scan parameter for image acquisition.

voltage kV	current µA	No. of projections	scan time hrs	voxel size mm	filter mm	source-object distance mm	object-detector distance mm
120	70	1080	0.93	0.048	0.5, Cu	189.3	311.7

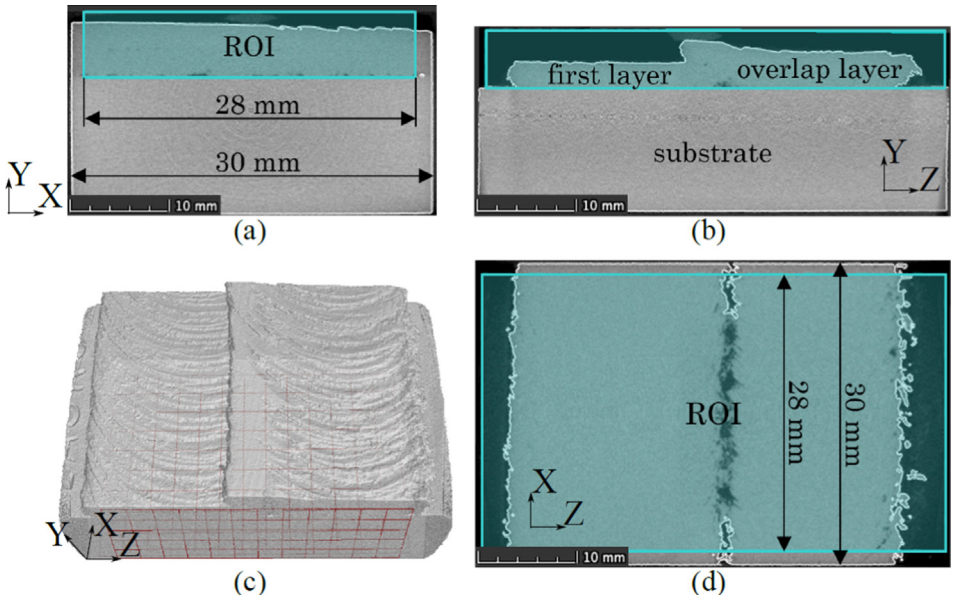

Fig. 5. Reconstructed microCT image data of an unmachined MTFS deposit in three different orientations (X/Y (a), Z/Y (b) and Z/X (d)) and a 3D rendering (c). In addition, the position and dimension of the region of interest - ROI (turquoise area) for the microCT-image based defect analysis is shown.

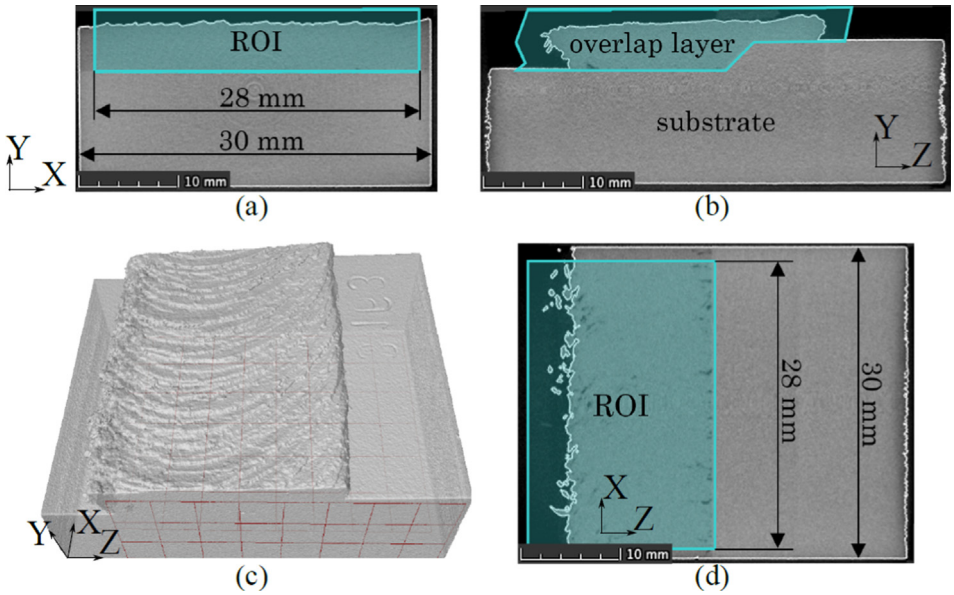

Fig. 6. Reconstructed microCT image data of a MTFS deposit with previous layer edge preparation in three different orientations (X/Y (a), Z/Y (b) and Z/X (d)) and a 3D rendering (c). In addition, the position and dimension of the region of interest - ROI (turquoise area) for the microCT-image based defect analysis is shown.

by Shinoda et al. [10]. According to the authors, during the deposition of the overlapping layer, the plasticized material at the tip of the consumable stud is transformed into two parts, in an upper and a lower part, which represents a key difference between single-track FS and multi-track FS. Due to the difference in height, the upper part of the interface has to sustain higher pressures, which may increase with increasing OD, since the layer edge tends to be closer to the center of the consumable stud. On the other hand, the axial force applied at the lower part decreases with increasing OD. Consequently, insufficient contact is achieved at the lower part of the interface and the plasticized consumable material is assumed to be deposited under shear stress only, resulting in an incomplete LTS-bonding and cold lap formation. Moreover, when overlapping with RS or AS, the different stress distribution as well as the flow direction of the plasticized material and the force distribution under the stud during deposition are

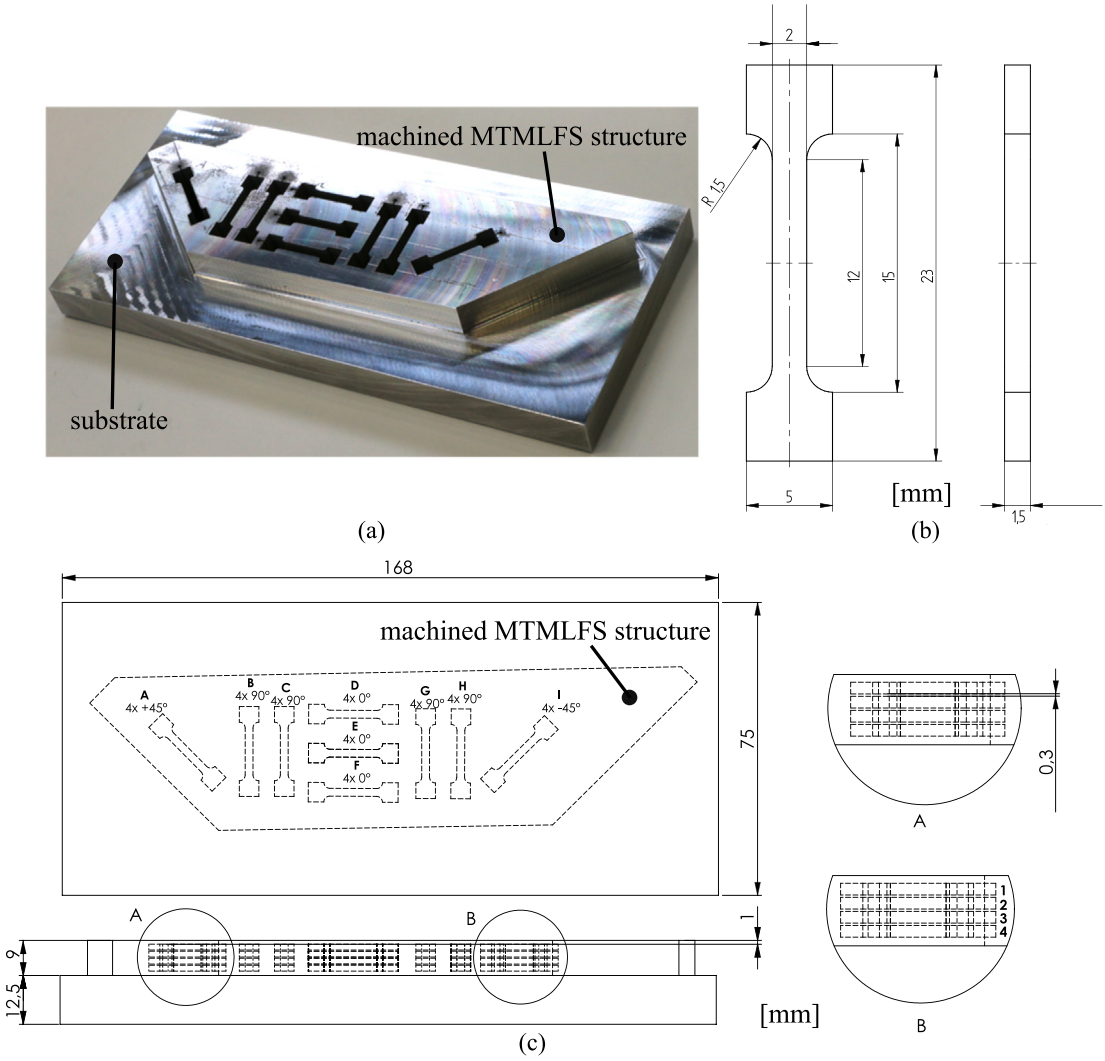

Fig. 7. Generated AA5083-H112 MTMLFS structure for the proposed block-style deposition scheme involving HFDB post-processing. The structure is shown after CNC machining and EDM extraction of MFTT specimens (a). Drawings of MFTT specimens (b) and schematic positioning of micro flat tensile specimens in MTMLFS layer stack.

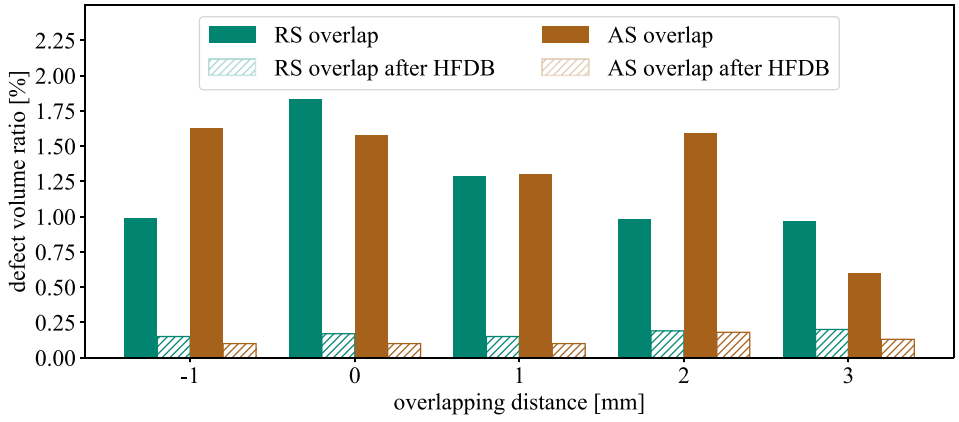

Fig. 8. Defect volume ratios of the individual unmachined multi-track friction surfacing deposits without and after HFDB post-processing, depending on the overlapping distance (OD) and the overlapping side (AS, RS).

considered to have an influence in this context. In general, an increase in OD towards the layer led to a decrease in defect volume ratio and a reduction of the distinct volumetric defect formation ("tunnel defect") in the overlapping area, however, no full consolidation could be achieved by this configuration. Still, due to the increasing frictional contact with increasing OD between the edge of the previously deposited track and the rotating stud while depositing the overlapping layer, improved inter-track bonding

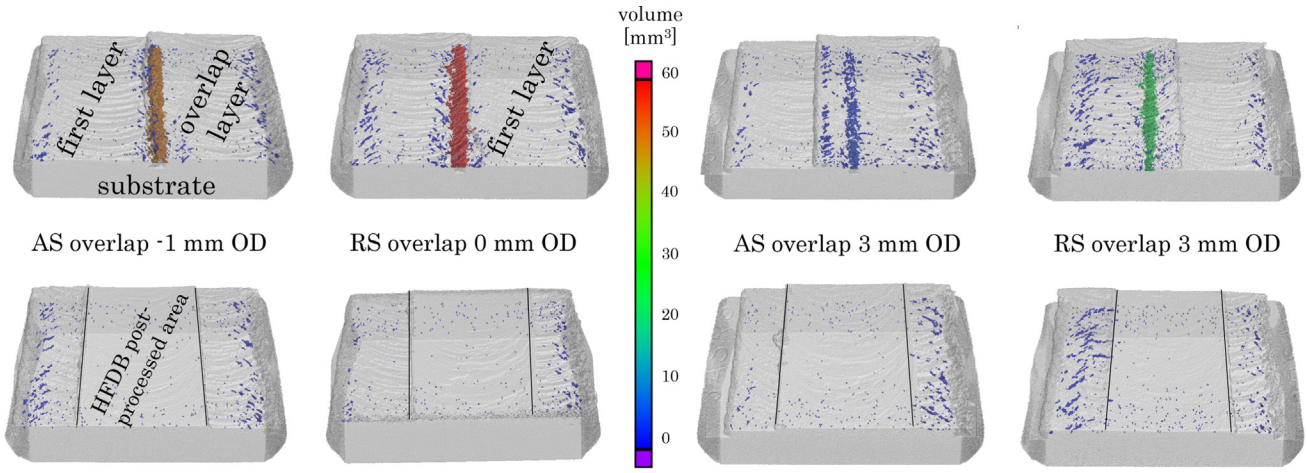

Fig. 9. Volumetric defect distributions for selected unmachined MTFS deposits with AS and RS overlap, depending on the OD without (top) and after (bottom) HFDB post-processing.

properties can be assumed [9]. However, if the OD is increased too much, LTS bonding might be incomplete for the resulting layer, since the stud is more in contact with the previously deposited layer than the substrate. For these reasons, it is necessary to investigate post-processing operations in the generation of MTFS deposits in order to achieve sound, defect-free metallurgical joints in the LTS and inter-track interfaces.

Effect of HFDB

In order to achieve defect-free inter-track and LTS-bonding of both layers, the suitability of HFDB post-processing for subsequent defect consolidation in the overlapping area is analyzed in the following. The obtained defect volume ratios for the generated unmachined MTFS deposits without and after HFDB post-processing are shown in Fig. 9. The results demonstrate that through HFDB post-processing in the overlapping area, a significant reduction in defect volume ratio of max. 93 % (RS overlap at 0 mm OD) could be achieved, yielding defect volume ratios between 0.1 % and 0.2 %, see Fig. 8. In general, higher defect volume ratios are obtained for RS[2] overlap compared to AS overlap after HFDB post-processing. This is caused by the higher volumetric defect formation in the LTS-interface and at the layer edges as indicated in Fig. 9 for RS overlap. The minimum measured defect volume ratio after HFDB post-processing is achieved for AS overlap at OD between −1 mm to 1 mm, measuring identical ratios of 0.1 %. The distinct volumetric defect formation in the overlapping area ("tunnel defect"), representing the majority of the total defect volume of the MTFS deposits, could be fully consolidated for both overlapping sides and at every OD via HFDB post-processing. Only some small defects in the main bonding area of the LTS-interface are identified, Fig. 9, measuring volumes in the range of the minimum detectable defect volume.

3.1.2. Prepared edges

Effect of angle and OD

In order to increase the bonding, a possible benefit of machining the unbonded part of the deposited layer to a defined shape before depositing the next layer is investigated in the following. In this regard, different edge preparations of the previously deposited layer are possible. To mimic possible edge preparations, a specially designed substrate is used, see Section 2.2. Since higher defect volumes were obtained with RS overlap, the further investigation of the process behavior on machined edges concentrates on AS overlap. The microCT-based defect analysis of this investigation focuses mainly on the deposits with OD of −1 mm and 2 mm.

The results of the measured defect volume ratios for different edge preparations are shown in Fig. 10. At −1 mm OD, the defect volume ratio tends to decrease with increasing outward bevel angle, with the minimum defect volume ratio of 0.11 % at 75° outward bevel angle. The highest defect volume ratio is observed for the right-angled edge preparation, where at 2 mm OD a significantly lower defect volume ratio (0.45 %) compared to −1 mm OD is measured. For 2 mm OD, the defect volume ratio remains approximately the same up to an outward bevel angle of 45° and then decreases further to a minimum of 0.21 % at 75°, which is slightly higher than for -1 mm OD. Due to the fact that the overlapping interface geometry approaches a planar surface with increasing angle, it is assumed that the transformation of the plasticized material into an upper and lower part becomes less pronounced, which causes a more balanced force distribution at the stud tip.

As can be seen by the volumetric defect distributions in Fig. 11, less volumetric defect formation occurred in the overlapping area, resulting in a nearly defect-free bonding to the prepared edge. Additionally, Fig. 12 depicts a detailed cross-sectional macrograph of the inter-track interfaces of a MTFS deposit with AS overlap at −1 mm and 2 mm OD for a right-angled shaped layer edge preparation. An increase in OD led to an increasing plastic deformation of the layer edge. This is usually more pronounced for AS overlap and is especially observed for right-angled and 15° outward bevel angle layer edge preparation.

The higher defect volume ratios for AS overlap at 2 mm OD compared to 1 mm OD for most outward bevel angles may be due to the rise in incomplete bonding in the LTS-interface and the more distinct cold lap formation with increasing OD, as observed for the unmachined MTFS deposits with high volumetric defects at the interface, see Fig. 9. The samples with outward bevel angle of 75° for AS overlap at both OD (2 mm and −1 mm) showed no volumetric defects in the overlapping area. Regarding the deposition efficiency, however, it should be noted that the effectively used deposited material would be reduced by approximately 25 % through subsequent machining of a layer edge with an outward bevel angle of 75°, even more when considering the cold laps.

Effect of HFDB

The defect volume ratios of the MTFS deposits for varied edge preparations after HFDB post-processing also exhibit a decreasing trend, Fig. 10. However, since the defect volumes for varied edge preparations without HFDB post-processing are already lower, the actual decrease is much less, but the nominal defect volume

[2] Please note again that AS and RS are transposed between FS and HFDB, where the specification of AS and RS always refers to the FS process.

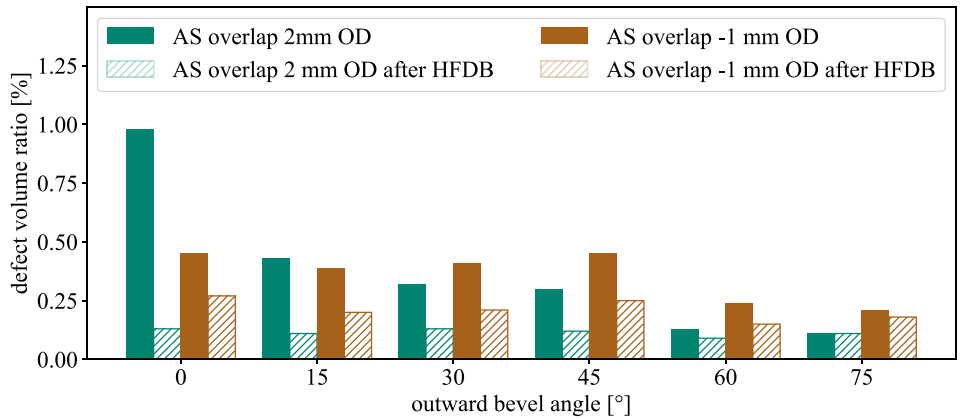

Fig. 10. Defect volume ratios of the individual overlapping layers for the MTFS deposits with AS overlap at ODs of 2 mm and −1 mm, without and after HFDB post-processing, depending on the layer edge preparation.

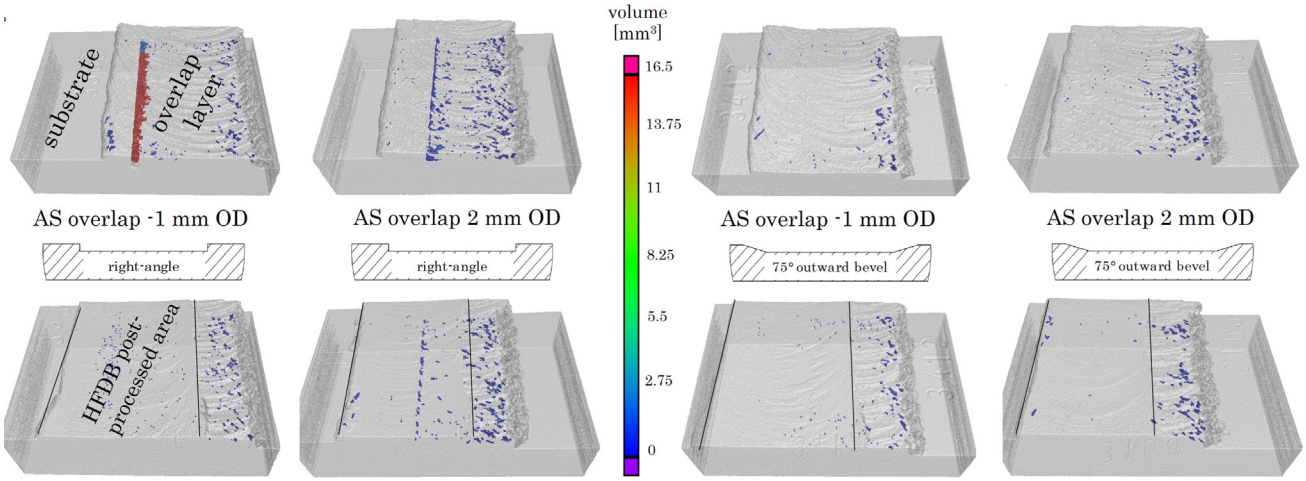

Fig. 11. Volumetric defect distributions for selected varying layer edge preparations for MTFS deposits with AS overlap at −1 mm and 2 mm OD.

ratios are comparable to unmachined MTFS deposits after HFDB post-processing, see Section 3.1.1. For instance, the post-processed HFDB samples for AS overlap at −1 mm OD are free of any significant volumetric defects in the overlapping area, except for a few small defects in the LTS-interface, which become less with increasing outward bevel angle, Fig. 11. At 2 mm OD with right-angled edge preparation, volumetric defects in the overlapping area can be found even after HFDB post-processing, which also decrease with increasing outward bevel angle until no significant volumetric defects in the overlapping area can be detected. Fig. 12c, d shows a detailed macrograph of the inter-track interfaces after HFDB post-processing the overlapping area. The induced severe plastic deformation in the overlapping region results in a defect-free, sound metallurgical bonding between the right-angled shaped edge and the deposited overlapping layer. Similar observations could also be observed for the other edge preparations, but not as pronounced as for the right-angled edge preparation.

The results show that edge preparation can have a very beneficial effect on the bonding, especially when HFDB is not applicable or feasible. The application of HFDB leads to similar defect volume rations for deposits on an unmachined layer and deposits on a prepared edge. Overall, the defect volume analysis showed that almost defect-free MTFS structures can be achieved when HFDB is applied, highlighting the broad potential of this process for the consolidation of any defect volumes, and thus ensuring sound, defect-free joints. The major benefit of the HFDB post-processing technique in comparison to machining the layer edges is that no material removal is necessary for achieving a sound, nearly defect-free metallurgical bond in the LTS-interface and between adjacent overlapping FS deposits. In terms of the generation of MTFS deposits, the HFDB process represents an efficient solution with respect to the effectively usable deposited material.

3.2. Feasibility for Additive Manufacturing

In the previous section, it was shown that by adapting OD and HFDB post-processing, defect-free deposition of multiple FS layers next to each other can be achieved, providing the possibility to coat larger surface areas without considerable volumetric defects. Although FS is still a discontinuous process, the knowledge on MTFS makes FS less dependent on the dimensions of the used consumable stud, i.e. the stud diameter is no longer the limiting factor for instance of the wall thicknesses for additively manufactured structures via FS.

The next step of FS for solid state AM is to build a structure with multiple layers on top and next to each other, i.e. MTMLFS. To the authors' information, the only approach for MTMLFS in the literature was performed by Dilip et al.[19] for steel who designed a MTMLFS structure consisting of five deposits next to each other for the first layer of the structure, four deposits in the second layer and three deposits in the third layer generating a pyramidal struc-

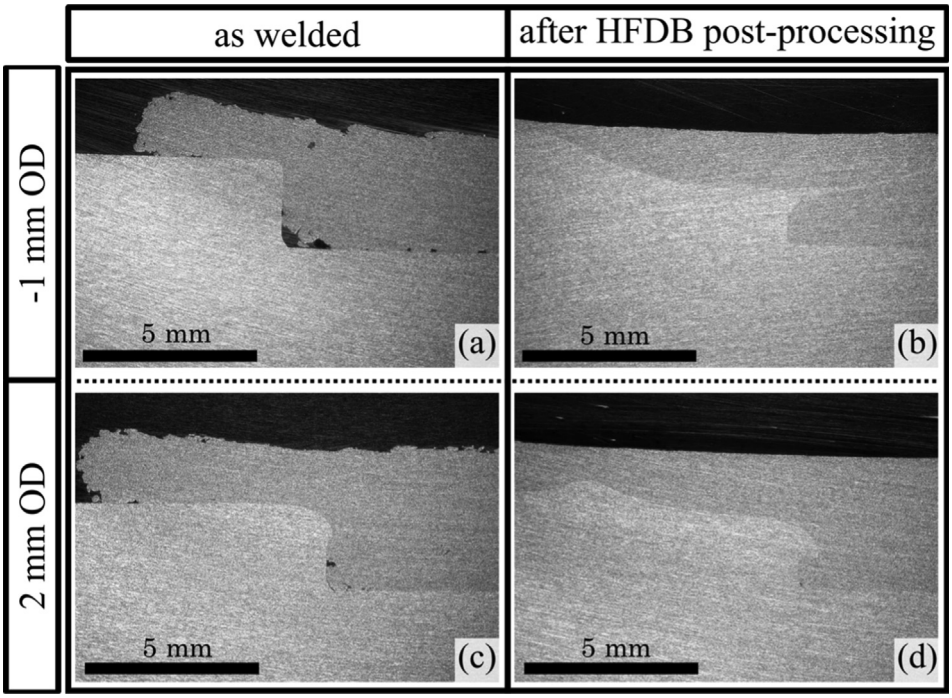

Fig. 12. Macrograph of inter-track interface in as welded condition and after HFDB post-processing, produced with AS overlap at −1 mm (a,b) and 2 mm (c,d) OD on a right-angled layer edge preparation.

ture. A similar pyramidal structure was built with the aluminum alloys used in this study. The cross section of this pyramid-style structure is shown in Fig. 13 (a).

Unlike the construction from mild steel by Dilip et al.[31], the volumetric defects in the overlapping area could not be consolidated through subsequent layer deposition. Therefore, large volumetric defects remain within the overall structure. In addition, the cold laps increase, causing defects in the LTS and LTL interfaces of the individual tracks and thus a decrease in the defect-free main bonding width. The difficulties in the process by applying this type of deposition scheme can be already found in the initial plasticizing phase, when depositing the middle and top layers. This is mainly due to the irregular and rough surface finish in the overlapping area of the underlying deposits, which makes the stud susceptible to buckling failure during plasticizing. For these reasons, the pyramidal approach was not further investigated.

The proposed MTMLFS approach in this study, including HFDB post-processing of the layers, is a block-style construction where the number of deposits is not changed along wall height of the structure. The applied manufacturing procedure is presented in Fig. 4. The cross section of this structure after machining is presented in Fig. 13b. No significant volumetric defects in the MTMLFS deposit can be identified, which was confirmed by 3D microCT scans. By applying the block-style deposition scheme, an optimized height-width ratio and a clearly defined overlapping area, beneficial for the determination of the inter-track bonding strength via MFTT, is achieved. Apart from this, HFDB post-processing ensures an even surface finish, preventing the stud from buckling during the initial plasticizing phase for subsequent FS processes. After machining, a basically defect-free MTMLFS structure with 40 mm in width and 10 mm in height could be achieved from eight FS layers. Consequently, approximately 60 % of the deposited material forms the defect-free bulk material[3]. In the following, the mechanical properties of the deposited layer material within the MTMLFS structure are investigated.

3.3. Tensile testing

Through MFTT, the ultimate tensile strength (UTS) as well as the yield strength ($R_{p0.2}$) and elongation at break (A) were determined. Fig. 14a exhibits the average values and standard deviations for the tested specimens with regard to their orientation in the built structure. For all tested specimens the overall average UTS is 303.7 MP a ± 18.8 MPa, matching the UTS of the AA5083 H112 base material (300 MPa [32]). The overall average yield strength, $R_{p0.2}$, is 157.9 ± 5.4 MPa which is approximately 17 % lower compared to the AA5083 H112 consumable stud base material (190 MPa [32]). The values for elongation at break, A, show a high deviation, which does not allow a sound investigation. Comparing the results for the different orientations, no significant directional dependency can be observed. However, the specimens extracted from positions closer to the interface to the AA2050 substrate tend to show slightly higher UTS values than the samples extracted from positions higher in the stack, Fig. 14b. From these results, a minimal gradient in UTS along the height of the deposited material was observed. This might be related to the application of subsequent thermo-mechanical processes, i.e. FS and HFDB. In this regard, the first layer experiences a higher number of thermo-mechanical cycles due to further FS deposits and HFDB processes. This might lead to a consolidation and possible additional strain hardening effects, especially of the first layers. In terms of $R_{p0.2}$, no relevant gradient was observed.

The high resolution microCT scans conducted in the gauge length for specimens, where early failure and thus lower tensile strength had been observed, are exemplary shown in Fig. 15. The extraction process by EDM is assumed to be one of the main causes for crack initiation leading to early failure. An example for this is given by two microCT image slices in the gauge length of one sample from Position C (261.4 MPa UTS), Fig.15. The slices show dis-

[3] The deposited structure was weighed before and after milling. The mass of the final structure (without the cold laps) is 60 % from the total deposited material mass.

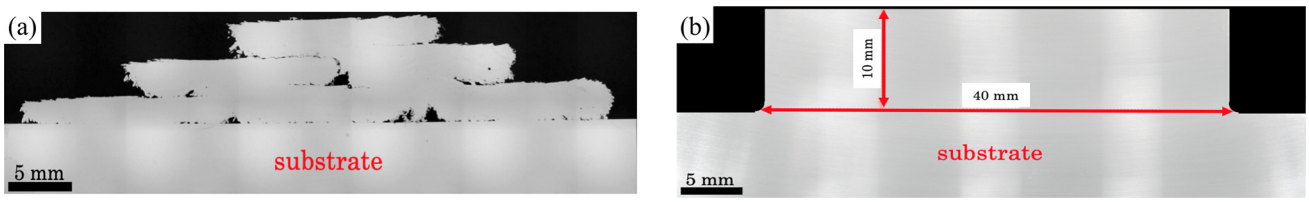

Fig. 13. Cross-sectional macrograph of pyramid-style construction (a) and generated multi-track multi-layer friction surfacing after CNC machining under application of block-style deposition scheme (b).

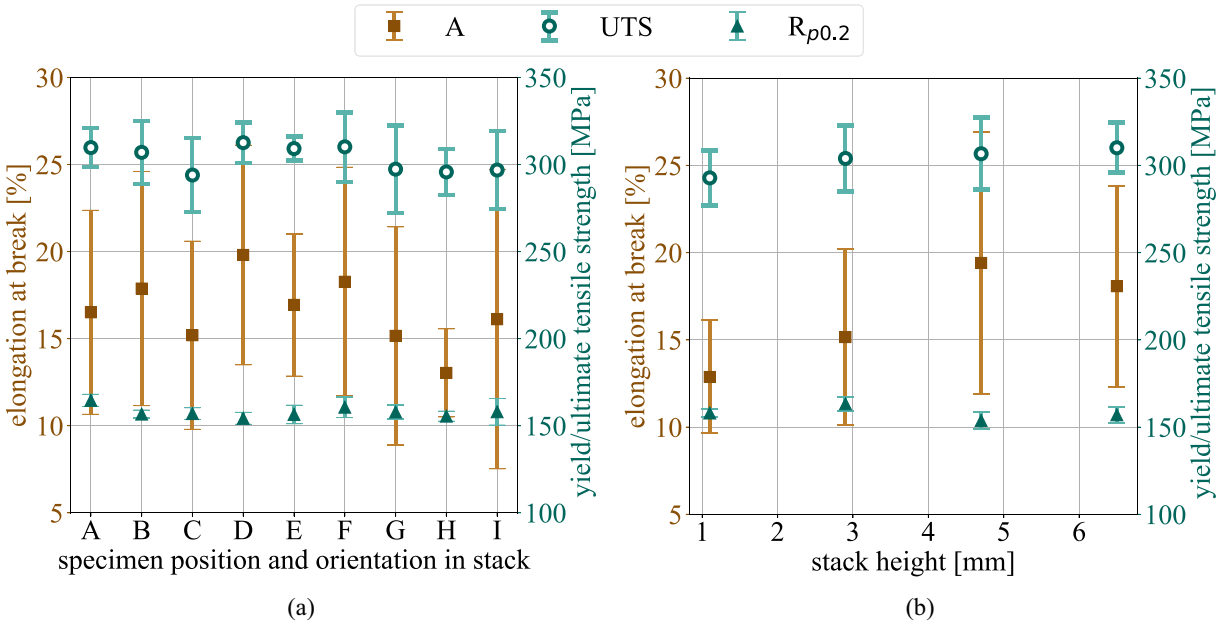

Fig. 14. Ultimate tensile strength (UTS), yield strength ($R_{p0.2}$) and elongation at break (A) for micro-flat tensile specimens analyzed with regard to position and orientation A-I (a), see Fig. 7, and height (b) in stack built by MTMLFS, including HFDB post-processing.

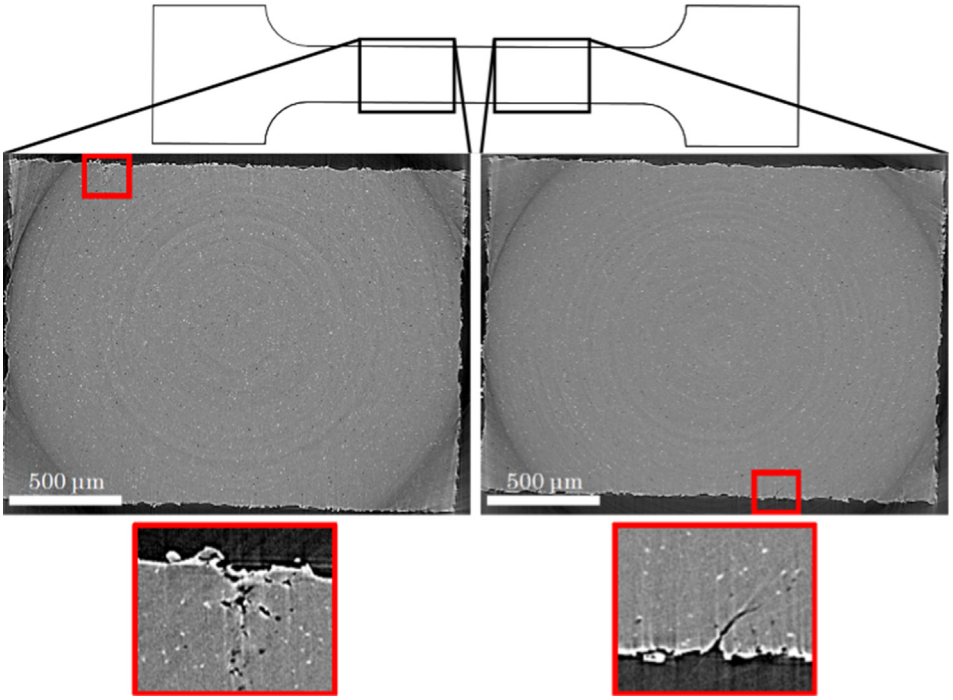

Fig. 15. MicroCT-image slice of MFTT specimen 3 of Position C in different positions within the gauge length. Distinct cracks near the specimen surface could be identified, which may be related to the EDM extraction process.

tinct cracks near the specimen surface in various positions within the gauge section before being tested. Since no other significant defects have been identified, the already uneven surface finish through the EDM process may be a reason for further outliers and high deviation, especially in terms of elongation at break.

Overall, the MFTT showed UTS values at least similar to the base material where no dependency on the orientation in the built stack could be observed. Considering the results shown in this work, multi-track FS of AA5083-H112 over AA2050-T84 substrates combined with HFDB post-processing represents a suitable candidate for large-scale coating or AM applications. Even for wide-area corrosion and wear protection applications, the multi-track FS approach in combination with the HFDB process is a promising solution. Moreover, the ability to join dissimilar aluminum alloys allows the manufacture of tailored structures, which makes FS to be considered as solid state AM technology for metals.

4. Conclusion

In the present work, multi-track FS overlap configurations were investigated for the deposition of AA5083- H112 over AA2050-T84 substrates. An extensive microCT-image based volumetric defect analysis was performed for all generated MTFS deposits. Apart from the effect of overlapping side, overlapping distance and the behavior on machined angled edges, HFDB post-processing has significant effect on the volumetric defect distribution. The main results of this study are summarized as follows:

- For both overlapping sides, an increase in OD led to a rise in incomplete bonding in the LTS-interface and cold lap formation. Additionally, a decrease in defect volume ratio with a reduction of the distinct volumetric defect formation ("tunnel defect") in the overlapping area was observed.
- The bonding might be enhanced by preparing the edge of the previously deposited layer with a large outward bevel angle.
- HFDB post-processing in the overlapping area led to a reduction of defect volume ratio of up to 93% and the most significant volumetric defects ("tunnel defect") could be fully consolidated, resulting in sound metallurgical bondings at the LTS interface and adjacent overlapping layers.
- The study has demonstrated that through the applied deposition scheme in combination with HFDB post-processing, a basically defect-free MTMLFS structure can be obtained. Micro-flat tensile specimens extracted from different positions and orientations of the deposited material did not reveal significant directional gradients, where the obtained strength is comparable to the stud base material.

With the obtained knowledge, large areas can be coated via MTFS and a further development of the approach MTMLFS is possible for AM structures. In summary, the deposition of aluminum alloys via FS combined with HFDB post-processing gives a good prospect on the potential and feasibility for large-scale AM applications.

5. Author Contributions

Conceptualization: Z.K., A.R., B.K.; Methodology: M.S., A.R.; Validation: M.S.; Formal analysis: M.S., Z.K.; Investigation: M.S.; Resources: B.K.; Data Curation: M.S., Z.K., B.Z.-P.; Writing - Original Draft: M.S., Z.K.; Writing - Review & Editing: M.S., Z.K., A.R., B.Z.-P., B.K.; Visualization: M.S., Z.K.; Supervision: A.R., B.K.; Funding: B.K.

6. Funding

B.K. acknowledges funding from the European Research Council (ERC) under the European Union's Horizon 2020 research and innovation programme (grant agreement No 101001567).

7. Data availability

The obtained data of this research is online available at Zenodo (DOI: 10.5281/zenodo.6592245).

Declaration of Competing Interest

The authors declare that they have no known competing financial interests or personal relationships that could have appeared to influence the work reported in this paper.

Acknowledgments

The authors would like to thank Mr. H. Tek from Helmholtz-Zentrum Hereon, Institute of Materials Mechanics-Laser Processing and Structural Assessment, for the support in conducting the tensile testing experiments. In addition, the authors want to thank Dr. Vasyl Mikhailovich Haramus of the Helmholtz-Zentrum Hereon, Institute of Metallic Biomaterials, for facilitating the micro-computed tomographic image acquisition. The authors would like to acknowledge the opportunity for microCT scans at the Manchester Imaging Branchline (I13-2), at Diamond Light Source UK.

References

[1] J. Gandra, H. Krohn, R.M. Miranda, P. Vilaça, L. Quintino, J.F. Dos Santos, Friction surfacing—a review, J. Mater. Process. Technol. 214 (5) (2014) 1062–1093.
[2] U. Suhuddin, S. Mironov, H. Krohn, M. Beyer, J.F. Dos Santos, Microstructural evolution during friction surfacing of dissimilar aluminum alloys, Metall. Mater. Trans. A 43 (13) (2012) 5224–5231.
[3] J. Ehrich, A. Roos, B. Klusemann, S. Hanke, Influence of mg content in al alloys on processing characteristics and dynamically recrystallized microstructure of friction surfacing deposits, Mater. Sci. Eng. A 819 (2021) 141407.
[4] S. Hanke, J.F. Dos Santos, Comparative study of severe plastic deformation at elevated temperatures of two aluminium alloys during friction surfacing, J. Mater. Process. Technol. 247 (2017) 257–267.
[5] H. Li, W. Qin, A. Galloway, A. Toumpis, Friction surfacing of aluminium alloy 5083 on DH36 steel plate, Metals 9 (4) (2019) 479.
[6] H. Klopstock, A.R. Neelands, An improved method of joining or welding metals, british patent specification 572789 (1941).
[7] M. Yu, H. Zhao, Z. Zhang, L. Zhou, X. Song, N. Ma, Texture evolution and corrosion behavior of the AA6061 coating deposited by friction surfacing, J. Mater. Process. Technol. 291 (2021) 117005.
[8] Y. Huang, Z. Lv, L. Wan, J. Shen, J.F. dos Santos, A new method of hybrid friction stir welding assisted by friction surfacing for joining dissimilar ti/al alloy, Mater. Lett. 207 (2017) 172–175.
[9] R. Puli, G.D. Janaki Ram, Microstructures and properties of friction surfaced coatings in AISI 440C martensitic stainless steel, Surf. Coat. Technol. 207 (2012) 310–318.
[10] T. Shinoda, J.Q. Li, Y. Katoh, T. Yashiro, Effect of process parameters during friction coating on properties of non-dilution coating layers, Surf. Eng. 14 (3) (1998) 211–216.
[11] S. Hanke, M. Beyer, A. Silvonen, J.F. Dos Santos, A. Fischer, Cavitation erosion of Cr60Ni40 coatings generated by friction surfacing, Wear 301 (1–2) (2013) 415–423.
[12] H. Tokisue, K. Katoh, T. Asahina, Structures and mechanical properties of multilayer friction surfaced aluminum alloys, Report of the Research Institute of Industrial Technology, Nihon University (2005).
[13] H. Tokisue, K. Katoh, T. Asahina, T. Ushiyama, Mechanical properties of 5052/2017 dissimilar aluminum alloys deposit by friction surfacing, Mater. Trans. 47 (3) (2006) 874–882.
[14] J.C. Galvis, P.H.F. Oliveira, J.d.P. Martins, A.L.M.d. Carvalho, Assessment of process parameters by friction surfacing on the double layer deposition, Mater. Res. 21 (3) (2018) 321.
[15] J. Gandra, P. Vigarinho, D. Pereira, R.M. Miranda, A. Velhinho, P. Vilaça, Wear characterization of functionally graded Al–SiC composite coatings produced by Friction Surfacing, Materials & Design 52 (2013) 373–383.

[16] S. Krall, C. Baumann, H. Agiwal, F. Bleicher, F. Pfefferkorn, Investigation of multilayer coating of EN AW 6060–T66 using friction surfacing, Journal of Machine Engineering 22 (2022).
[17] J. Shen, S. Hanke, A. Roos, J.F. Dos Santos, B. Klusemann, Fundamental study on additive manufacturing of aluminium alloys by friction surfacing layer deposition, AIP Conf. Proc. 2113 (2019) 10015.
[18] E.S. Abdelall, A.F. Al-Dwairi, S.M. Al-Raba'a, M. Eldakroury, Printing functional metallic 3d parts using a hybrid friction-surfacing additive manufacturing process, Progress in Additive Manufacturing 10 (3) (2021) 103.
[19] J.J.S. Dilip, S. Babu, S.V. Rajan, K.H. Rafi, G.D. Janaki Ram, B.E. Stucker, Use of friction surfacing for additive manufacturing, Mater. Manuf. Process. 28 (2) (2013) 189–194.
[20] J. dos Santos, A. Roos, Process and device for producing a weldment between the surfaces of two flat workpieces with total running of the contacting surfaces of the friction stir tool into the surface of the second workpiece opposing the first workpiece. 2006, European Patent EP 1 769 877 B1 (2006).
[21] V. Fitseva, H. Krohn, S. Hanke, J.F. Dos Santos, Friction surfacing of Ti–6Al–4V: Process characteristics and deposition behaviour at various rotational speeds, Surf. Coat. Technol. 278 (2015) 56–63.
[22] J. Gandra, D. Pereira, R.M. Miranda, P. Vilaça, Influence of Process Parameters in the Friction Surfacing of AA 6082–T6 over AA 2024–T3, Procedia CIRP 7 (2013) 341–346.
[23] F.Y. Isupov, O. Panchenko, L. Zhabrev, I. Mushnikov, E. Rylkov, A.A. Popovich, Finite Element Simulation of Temperature Field during Friction Surfacing of Al-5Mg Consumable Rod, Key Eng. Mater. 822 (2019) 737–744.
[24] Z. Kallien, L. Rath, A. Roos, B. Klusemann, Experimentally established correlation of friction surfacing process temperature and deposit geometry, Surf. Coat. Technol. 397 (2020) 126040.
[25] J.P. Bergmann, F. Petzoldt, R. Schürer, S. Schneider, Solid-state welding of aluminum to copper-case studies, Welding in the World 57 (4) (2013) 541–550.
[26] A. Du Plessis, C. Broeckhoven, A. Guelpa, S.G. Le Roux, Laboratory x-ray micro-computed tomography: a user guideline for biological samples, Gigascience 6 (6) (2017).
[27] I.. A. E1441-11, Standard Guide for Computed Tomography (CT) Imaging, ASTM International, West Conshohocken, PA, 2011.
[28] V.G. GmbH, Reference Manual VGSTUDIO MAX 3.2, Volume Graphics GmbH (2019).
[29] A. Du Plessis, I. Yadroitsev, I. Yadroitsava, S.G. Le Roux, X-ray microcomputed tomography in additive manufacturing: a review of the current technology and applications, 3D Print, Addit. Manuf. 5 (3) (2018) 227–247.
[30] D. Dobi, E. Junghans, Determination of the tensile properties of specimens with small dimensions, Kovine Zlitine Tehnologije(Slovenia) 33 (6) (1999) 451–457.
[31] J.J.S. Dilip, G.D. Janaki Ram, B.E. Strucker, Additive manufacturing with friction welding and friction deposition processes, Int. J. Rapid Manuf. 3 (1) (2012) 56–69.
[32] MatWeb - Material Property Data, Aluminum 5083–H112 (Accessed 28.02.2022). http://www.matweb.com/search/DataSheet.aspx?MatGUID=bd6317b19dd94faf8bff851e4f339e88.